RADIO SCIENCE, VOL. 41, RS6001, doi:10.1029/2005RS003298, 2006

Characterization of terminal impedance and radiation properties of a horizontal VLF antenna over Antarctic ice

T. W. Chevalier,[1] U. S. Inan,[1] and T. F. Bell[1]

Received 10 June 2005; revised 22 March 2006; accepted 5 June 2006; published 17 November 2006.

[1] Measurements of the input impedance of two very low frequency (VLF) transmitters in Antarctica are used to validate existing dielectric models for the ice substrate at these frequencies. Using a finite difference time domain approach, Maxwell's equations are solved in the presence of dispersive media, representing the layers of ice which form the Antarctic ice sheet as a single-pole Debye material. This model provides simulated input impedance values in good agreement with measured data for both the South Pole beacon and the former Siple Station VLF transmitters. Using the validated simulation tool, the radiation characteristics of the South Pole beacon VLF transmitter are characterized. Results for the radiation resistance, efficiency, and far-field pattern are provided for the current South Pole transmitter. The power pattern for a two-element array is also determined.

Citation: Chevalier, T. W., U. S. Inan, and T. F. Bell (2006), Characterization of terminal impedance and radiation properties of a horizontal VLF antenna over Antarctic ice, *Radio Sci.*, *41*, RS6001, doi:10.1029/2005RS003298.

1. Introduction

[2] Over the past few decades, there has been interest in the study of VLF wave propagation within the Earth-ionosphere waveguide in the Antarctic region. For instance, *Cotton et al.* [1992] and *Reznikov et al.* [1993] studied the effects of the ionosphere on attenuation and polarization changes for VLF waves propagating over the Antarctic terrain. *Carpenter et al.* [1988] and *Helliwell and Katsufrakis* [1974] used the former Siple Station transmitter as a VLF wave injection instrument to probe regions of the ionosphere and magnetosphere. In addition, *Tkalcevic* [1983] compares measured data with results from a ray optics analysis for VLF waves propagating from Siple Station to Palmer Station, Antarctica.

[3] At the present time little is known about the electrical properties of the subsurface of the Antarctic plateau, consisting of layers of ice and snowpack with varying density and temperature. These properties can have a significant effect on the terminal loading and radiation properties of antennas placed above the subsurface, as well as on the propagation of signals in the VLF frequency range. Measurements of the terminal properties of an antenna thus offer the means to assess the properties of the ice, as we undertake to do herein.

[4] One of the first efforts to determine the characteristics of Antarctic ice was made by *Gow et al.* [1968]. *Gow et al.* [1968] collected data on the first ice core samples extending from the surface to the bedrock at a location near Byrd Station, Antarctica. Using this data, *Peden and Webber* [1970], approximating both the ionosphere and the ground as a lossy dielectric, modeled the subterrain with a bulk permittivity of $\epsilon_r = 6 - j14$ to obtain reflection coefficients as a function of incidence angle for Earth-ionosphere waveguide propagation. The motivation for that work was to provide an adequate representation for the fields radiated from a 34 km antenna buried in the snow at Byrd Station, Antarctica [*Peden et al.*, 1972]. *Webber and Peden* [1971] took this work one step further and included the effects of the ionosphere. With the ionosphere included, attenuation and polarization changes for both quasi–transverse electric and quasi–transverse magnetic modes were calculated using daytime and nighttime ionospheric conditions through the use of an anisotropic reflection coefficient derived from cold plasma theory. As in the case of *Peden and Webber* [1970], only far-field measurements at remote locations were available to validate the models. More recently, *Reynolds* [1985] performed a detailed analysis concerning the complex permittivity of the ice

[1]Department of Electrical Engineering, Stanford University, Stanford, California, USA.

0048-6604/06/2005RS003298$11.00

surface in Antarctica over a wide range of frequency and temperature conditions at select locations.

[5] Until the work of *Raghuram et al.* [1974], little effort had been made to determine the effects of the ice on near-field antenna performance. *Raghuram et al.* [1974] developed an ice model using the work of *Auty and Cole* [1952], in conjunction with existing ice core samples taken by *Gow et al.* [1968], in order to characterize various radiation characteristics of the Siple Station transmitter. *Auty and Cole* [1952] estimated the dielectric properties of ice across a range of temperatures by approximating the electrical characteristics of ice as a single-pole Debye material. *Raghuram et al.* [1974] used this data to develop a five-layer model for the ice profile below Siple Station in terms of its electrical characteristics. It was assumed that the relative dielectric constant of the ice varied from $3.05-j7.16$ for the layer between 10 and 1000 m to $14.60-j34.74$ for the layer just above the bedrock at 1900 m. Using the method of variations, *Raghuram et al.* [1974] varied their dielectric model until reasonable agreement was obtained with measured data for the input impedance of the transmitter.

[6] This paper concerns the numerical simulation of the terminal properties and radiation characteristics of horizontal dipole antennas on Antarctic ice, considering in particular the specific cases of the Siple Station VLF antenna operating at ~5 kHz [*Raghuram et al.*, 1974] and a new antenna at the South Pole operating at 19.4 kHz. Our first goal is to validate the use of existing dielectric models in ascertaining the radiation properties of VLF antennas operating over the Antarctic plateau. Our second goal is to provide a tool for extending this analysis to a multiple-antenna system and for analyzing the general problem of wave propagation through the Earth-ionosphere waveguide. The tool is based on the finite difference time domain (FDTD) method [*Yee*, 1966] and is discussed in detail in the following sections.

2. Simulation Characteristics

2.1. Ice Profile

[7] In previous studies of VLF antennas operating in the Antarctic environment, the major unknown has been the properties of the ice below the surface. Suitable approximations were often made to ease the computational burden [*Peden and Webber*, 1970; *Webber and Peden*, 1971]. Both studies suggested using bulk values of $6-j14$ for the relative dielectric constant. *Raghuram et al.* [1974] suggested the use of a more detailed ice model by partitioning the ice into a series of five stratified layers in each of which the relative dielectric constant was assumed to have the fixed value $\epsilon_n = \epsilon_n' + j\epsilon_n''$, where $n = 1.5$. The fixed value of ϵ_n for each layer was determined using density and temperature profiles fitted to a Debye material relation. The model of *Raghuram et al.* [1974] was a frequency domain approach which utilized available ice data at a frequency of 12.8 kHz. Since the ice core samples were not taken at Siple Station, the available ice measurements from *Gow et al.* [1968] were fit to the conditions of Siple Station, where the layer of bedrock was assumed to be at a depth of 1900 m. The bedrock was modeled as a conductor with a constant $\epsilon' = 10$ and $\sigma_{eff} = \omega\epsilon'' = 10^{-3}$ mho/m across all frequencies. Our model will follow the lead of *Raghuram et al.* [1974] and will assume that the ice-snow mixture below the Antarctic surface is well modeled by a single-pole Debye material given by

$$\epsilon' - i\epsilon'' = \epsilon_\infty + \frac{\epsilon_s - \epsilon_\infty}{1 + i\omega\tau}, \tag{1}$$

where ω is the radian frequency, ϵ_s is the permittivity of ice at zero frequency, ϵ_∞ is the permittivity at infinite frequency, and τ is the relaxation time constant. Although the data of *Gow et al.* [1968] were taken at Byrd Station, we use this profile, suitably modified, to accurately reflect the depths found at both Siple and South Pole stations through interpolation and extrapolation of the temperature and density data to match the respective geographic locations. It is assumed that the ice core samples taken by *Gow et al.* [1968] accurately reflect the consistency of the ice in different regions in Antarctica appropriately modified for depth. The primary assumption that is made in this work, as it pertains to the ice modeling, is that at a depth of about 2100 m, the density of the ice-snow mixture approaches that of pure ice; thus $\epsilon_r = \epsilon' - j\epsilon''$ has a maximum value beyond this depth.

2.2. Modeling Techniques

[8] The method chosen for our numerical simulation is FDTD, which is commonly used for the purpose of modeling transient electromagnetic phenomena in complex inhomogeneous media. FDTD is inherently a time domain approach; therefore the dispersive properties of the ice (i.e., the Debye response) must be accounted for in the time domain. FDTD provides the capability to model an arbitrarily fine material profile, with the numerical accuracy being limited only by the desired cell size and memory used for modeling both the ice and the antenna.

[9] The FDTD method has previously been used to determine the surface impedance of a lossy earth [*Thiel and Mittra*, 1997], but the work presented here represents one of the first applications of FDTD in modeling VLF wave propagation over Antarctic ice. The FDTD technique as applied to our ice model consists of solving the following system of first-order differential equations,

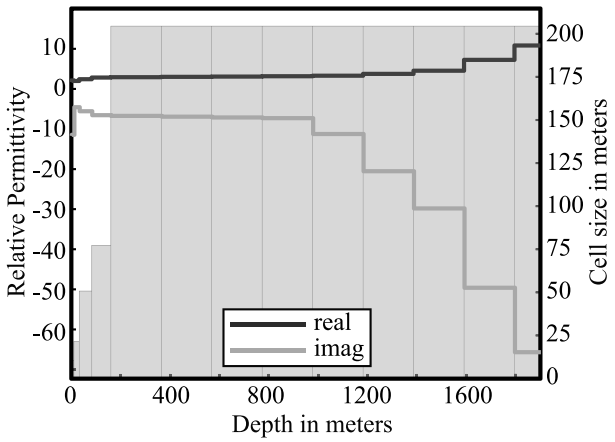

Figure 1. Variation of real and imaginary parts of ϵ_r with depth and cell size at 12.8 kHz for ice below Siple Station.

with equation (4) accounting for the currents induced in the ice.

$$\nabla \times \mathbf{H} = \epsilon_o \epsilon_\infty \frac{d\mathbf{E}}{dt} + \sigma \mathbf{E} + \mathbf{J_d} \tag{2}$$

$$\nabla \times \mathbf{E} = -\mu_o \frac{d\mathbf{H}}{dt} \tag{3}$$

$$\mathbf{J_d} + \tau \frac{d\mathbf{J_d}}{dt} = \epsilon_o (\epsilon_s - \epsilon_\infty) \frac{d\mathbf{E}}{dt}, \tag{4}$$

where $\mathbf{E}$ and $\mathbf{H}$ represent the wave electric and magnetic fields, $\mathbf{J_d}$ represents the current in the ice due to the

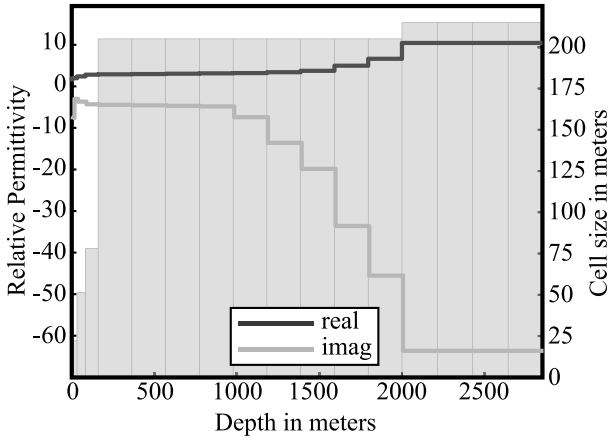

Figure 2. Variation of real and imaginary parts of ϵ_r with depth and cell size at 19.4 kHz for ice below South Pole Station.

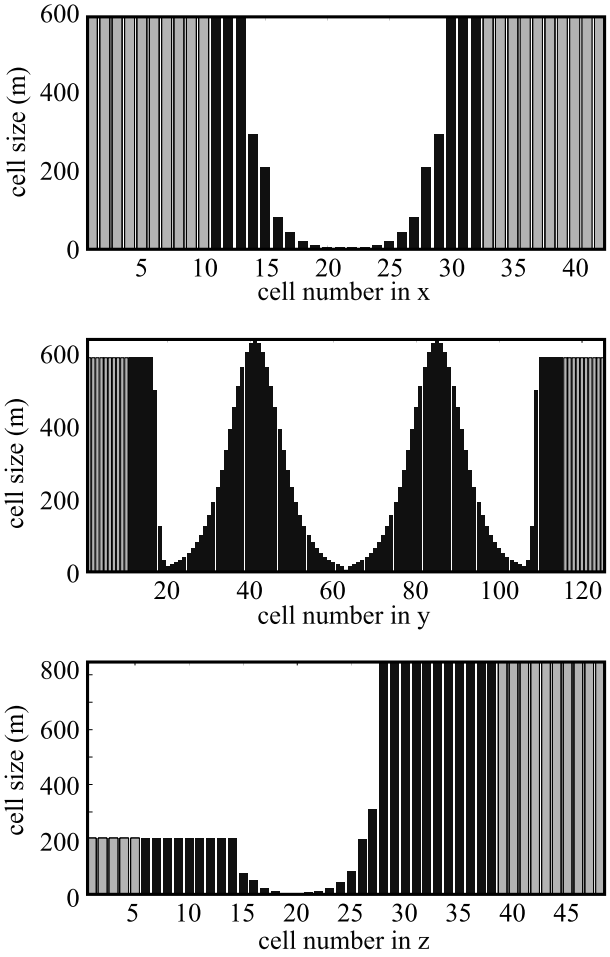

Figure 3. Nonuniform mesh used in Siple Station calculation with number of cells including PML layers $(x,y,z) = 42 \times 125 \times 48$. Black cells represent the computational domain, and gray cells represent the PML layers.

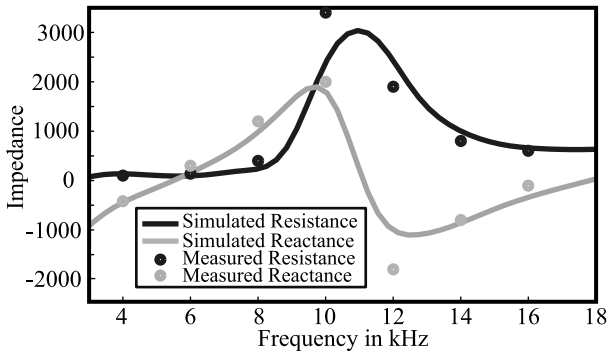

Figure 4. Calculated versus measured input impedance for the Siple Station transmitter.

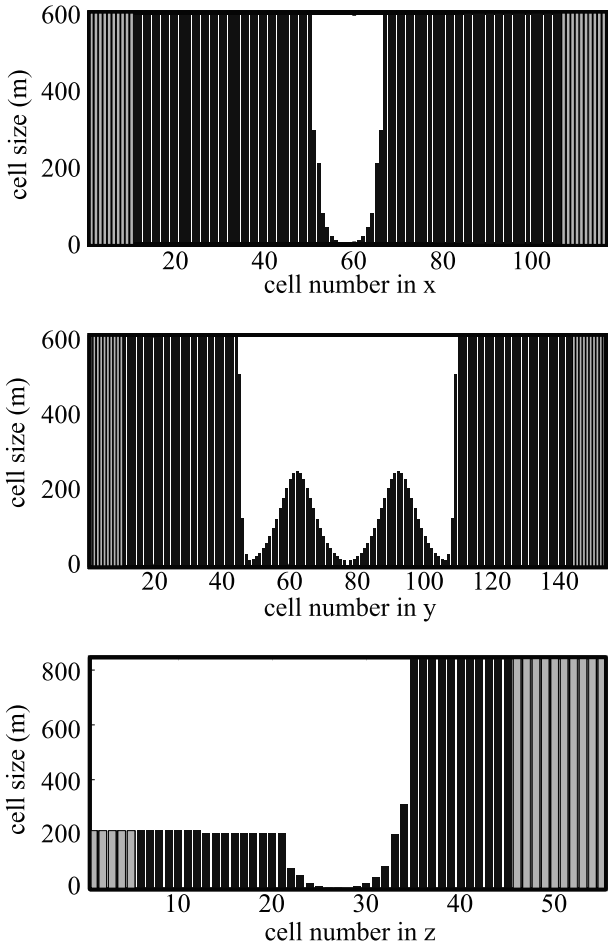

Figure 5. Nonuniform mesh used in South Pole beacon calculation. The number of cells including PML layers $(x,y,z) = 116 \times 153 \times 55$. Black cells represent the computational domain, and gray cells represent the PML layers.

Debye pole, σ is the conductivity, and ϵ_o and μ_o are the free space permittivity and permeability, respectively. Equation (4) is derived from equation (1) and Ampere's law by solving for the portion of the displacement current due to the Debye pole. This procedure results in the additional terms found in equation (2).

[10] Using the ice core data collected at a frequency of 12.8 kHz from *Gow et al.* [1968] in conjunction with the tabulated results for the dielectric properties of ice given by *Auty and Cole* [1952], we extract the necessary Debye parameters for the ice in the time domain, namely, ϵ_s, ϵ_∞ and τ.

[11] The antenna simulations presented in this paper apply to the long horizontal antenna above-ice configurations used at Siple Station and at the South Pole, where the ice thickness differs by about 1 km. At Siple Station, the layer of bedrock is assumed to be at a depth of 1900 m, while at the South Pole it is at 2850 m. Beyond these two respective depths, the material is assumed to be bedrock with $\epsilon' = 10$ and $\sigma_{eff} = \omega\epsilon'' = 10^{-3}$ mho/m as in the work by *Raghuram et al.* [1974]. The dielectric properties for the final ice model used in both the Siple Station and South Pole antenna simulations are given in Figures 1 and 2. Only the layers between the ice surface and the bedrock are shown.

[12] The gray vertical bars in Figures 1 and 2 represent the cell sizes as a function of depth. The ice profile located below each transmitter is divided into 14 and 18 layers for Siple Station and South Pole Station, respectively. As shown in Figures 1 and 2, the complex permittivity is assumed to be constant within each cell, and the permittivity of the ice at infinite frequency ϵ_∞ is equal to 1.0. The ice profile shown in Figure 1 allows for a greater variation in the dielectric parameters over the five-layer profile used by *Raghuram et al.* [1974]. Though it has been shown that pressure melting exists for layers in the ice that lie just above the bedrock

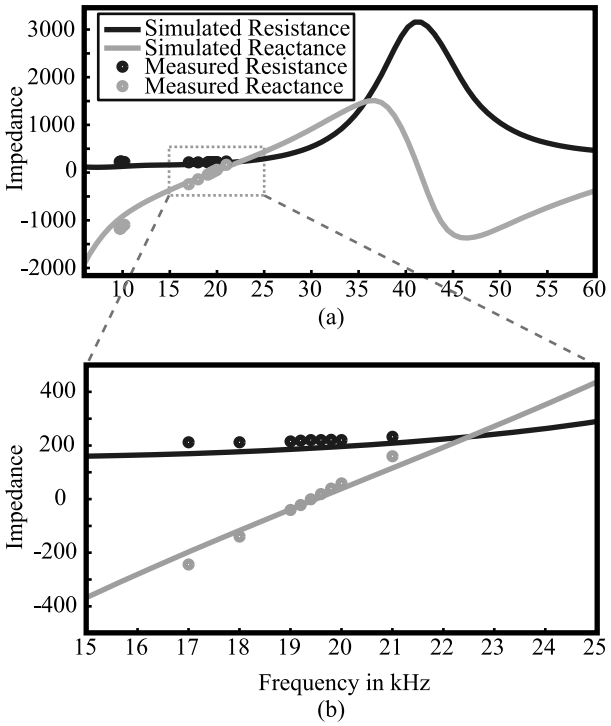

Figure 6. Calculated versus measured input impedance for the South Pole beacon transmitter: (a) broadband response and (b) expanded region around the resonant frequency point.

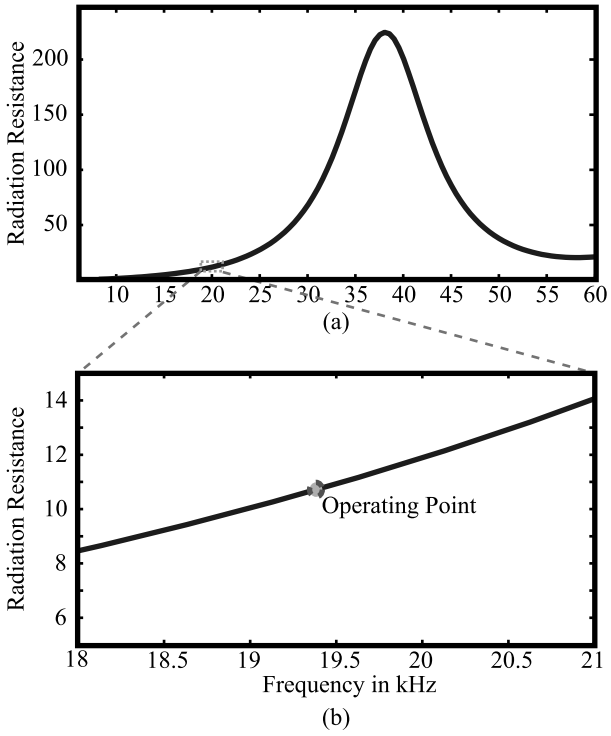

Figure 7. Radiation resistance: (a) broadband response and (b) expanded region around the resonant frequency point.

[*Rogers and Peden*, 1975; *Gow et al.*, 1968], the change in the dielectric properties of the fluid mixture over the thickness of this layer at VLF frequencies would be negligible and is therefore not included in the profiles of Figures 1 and 2.

[13] The VLF beacon transmitter at the South Pole operates at a frequency of 19.4 kHz. Since the ice permittivity data is only available at a frequency of 12.8 kHz, we use the Debye relation of equation (1) in conjunction with this data set to extract the dielectric properties at a frequency of 19.4 kHz. *Raghuram et al.* [1974] suggest adding a small conductivity of $5e^{-6}$ mho/m to account for impurities in the ice. This value, however, turns out to be orders of magnitude less than the imaginary part of the dielectric constant at VLF frequencies and can be safely neglected for the dielectric profiles at both Siple Station and at South Pole Station. It is assumed for the purpose of this model that the ionosphere has little effect upon the near-field properties of the two antennas at the frequencies of interest and is thus not included in our simulations.

[14] In both simulations, the computational domain utilizes a perfectly matched layer (PML) to absorb outgoing waves [*Berenger*, 1994]. The PML implementation presented in this work utilizes a convolutional PML based on work by *Chevalier and Inan* [2004]. All simulations were performed on a 28 node Beowulf cluster with run times on the order of 1–2 days with respect to the smallest and largest computational spaces.

3. Siple Station Comparison

[15] Our first case study compares measured data with the simulated input impedance of the Siple Station transmitter antenna. Since data for Siple Station are available over a wide frequency band, this case provides a good test of the efficacy of the model.

[16] The computational space (not including PML layers) is $22 \times 105 \times 33$ cells representing a region of space which is $10 \times 30 \times 12.1$ km in dimension with $0 \leq x \leq 10$ km, $0 \leq y \leq 30$ km, and $-2.1 \leq z \leq 10$ km. The 21.4 km dipole antenna, which represents the Siple transmitter, is oriented in the $\hat{y}$ direction, possessing a 4 m gap and located 4 m above the ground. The $\hat{z}$ direction corresponds to altitude. The antenna is excited with a resistive voltage source [*Piket-May et al.*, 1994] utilizing a 50 kHz bandwidth Gaussian pulse modulated at 20 kHz. In order to capture the small-scale features of the problem, a nonuniform mesh is used. The variation in cell size with respect to each coordinate direction is shown in Figure 3.

[17] The minimum cell size in Figure 3 is 4 m, and the maximum cell size within the ice is 600 m. The cell size in the vertical direction gradually increases from 4 m at the ice surface to a maximum of 200 m at the ice-bedrock interface. The axis of the antenna is represented by the middle plot in Figure 3, where the minima correspond to the gap and tips of the antenna. The minima in the top and bottom plots of Figure 3 represent the width of the antenna and location of the antenna-ice interface, respectively. Above the antenna in the $\hat{z}$ direction, the cell size

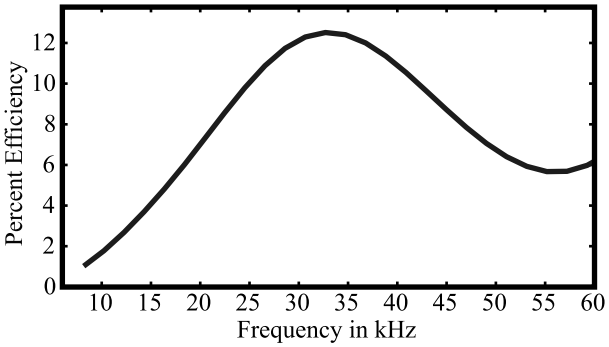

Figure 8. Radiation efficiency.

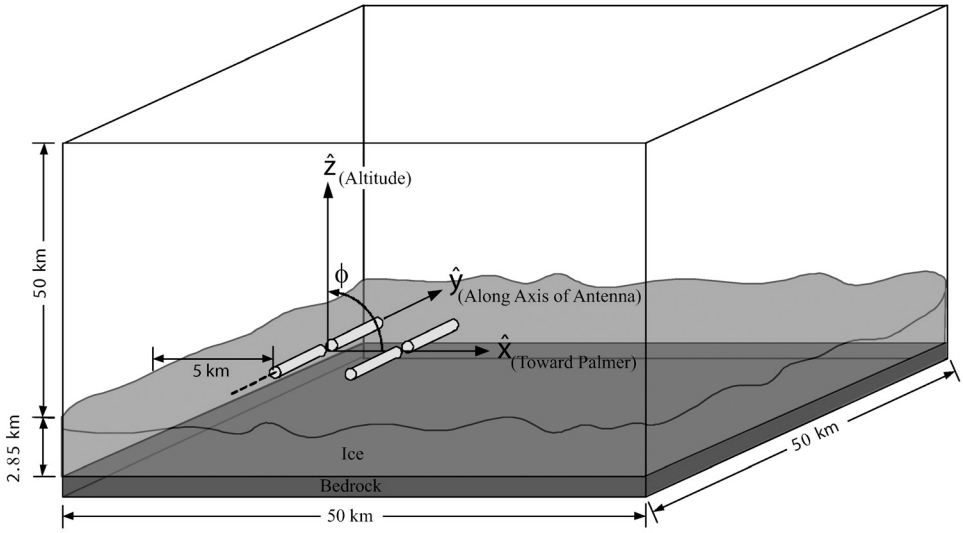

Figure 9. Conceptual diagram of simulation region for one- and two-element cases at South Pole Station.

increases to approximately 800 m. A thin wire approximation [*Taflove and Hagness*, 2000, pp. 420–423] is used to account for the 1 cm wire diameter of the Siple Station transmitter antenna. The computational space is truncated with a PML consisting of 10 layers in all directions (except for 5 layers below the bedrock interface). The simulation is run for 500 μs, allowing for the transients to subside so as to produce an accurate frequency response in the Fourier domain. Figure 4 represents the input impedance calculated by taking the ratio of the Fourier transformed currents and voltage at the terminals of the antenna:

$$Z_{in} = \frac{V(f)}{I(f)} = \frac{\mathcal{F}\left(\int \mathbf{E} \cdot dl\right)}{\mathcal{F}\left(\oint \mathbf{H} \cdot dl\right)}, \tag{5}$$

where $\mathcal{F}$ denotes the Fourier transform. As demonstrated in Figure 4, good agreement is obtained with the antenna input impedance measurements at Siple Station as given by *Raghuram et al.* [1974]. The simulated resonant frequency point is 5.5 kHz compared with the measured value of 5.1 kHz. The primary purpose of the comparison of our model results with the case of the Siple Station transmitter is to provide reassurance that both the ice model and the simulation are valid in this regime for a case where measured data are available. Slight adjustments in the model, such as modifications to the ice profile, allow for a more accurate comparison with the measured data; however, the point illustrated here is that unlike the work of *Raghuram et al.* [1974], the ice profile is derived directly from the data and is not adjusted until a suitable match is made with the measurements. This feature allows the model to be situation independent and validates the degree to which the ice model realized from the core samples represents Antarctic ice in other regions of the continent.

4. South Pole Beacon Comparison

[18] The South Pole beacon VLF transmitter is a recent system constructed in 2002. Our second case study compares the simulation model results with the available measured data on the transmitter input impedance, since this quantity can be directly measured. Assuming a reasonable match is made with the input impedance,

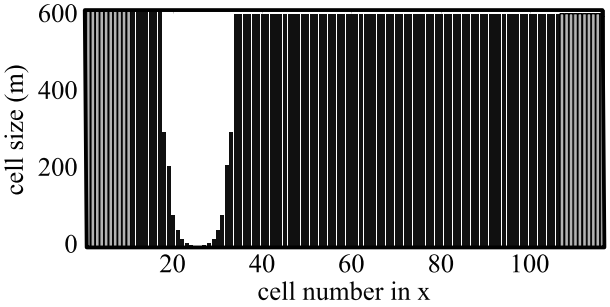

Figure 10. Nonuniform mesh in the $\hat{x}$ direction for the single-transmitter pattern. The antenna is 5 km from the edge of the space. The number of cells including PML layers $(x,y,z) = 116 \times 153 \times 100$. Black cells represent the computational domain, and gray cells represent the PML layers.

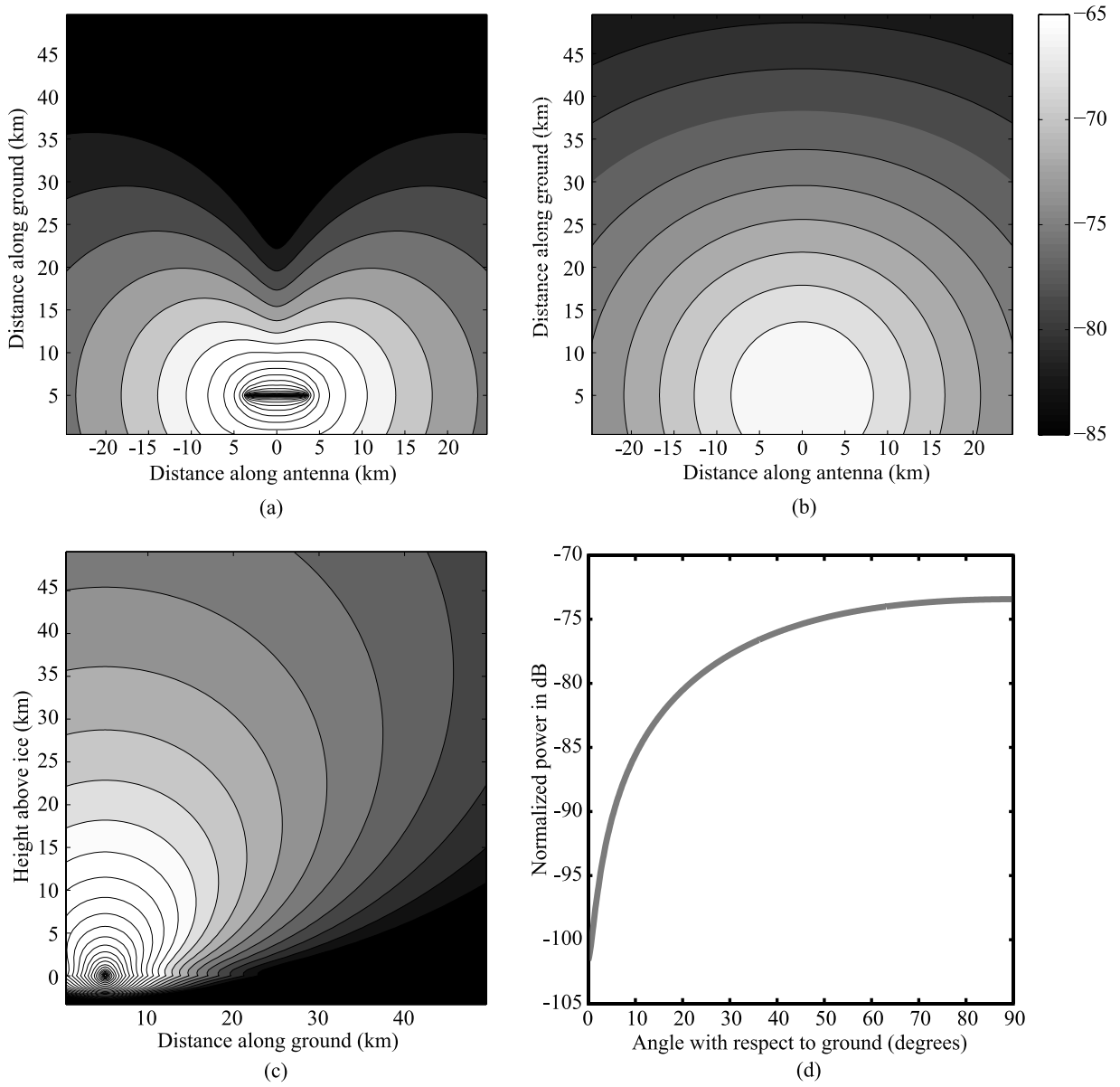

Figure 11. Normalized radiation pattern of the South Pole beacon in dB. (a) Power pattern in horizontal plane just above the ice surface. (b) Power pattern in horizontal plane at 15 km altitude. (c) Power pattern in vertical plane through antenna terminals. (d) Angular dependence of the power pattern at radial distance of 45 km from antenna terminals.

other simulated properties such as radiation resistance and pattern, which are much more difficult to directly measure, can be accurately determined.

[19] The surface of the ice at the South Pole is at an elevation of 2850 m above the bedrock. Ice core samples are not available to produce an accurate map of the ice profile below South Pole Station. Because of the lack of ice core data, we assume that the density of the ice-snow mixture at the limit of available measurements (∼2100 m) approaches that of pure ice. Beyond this depth, we simply cap the real and imaginary parts of the permittivity as shown in Figure 2.

[20] Input impedance measurements for the South Pole beacon are only available over a 10 kHz band, including

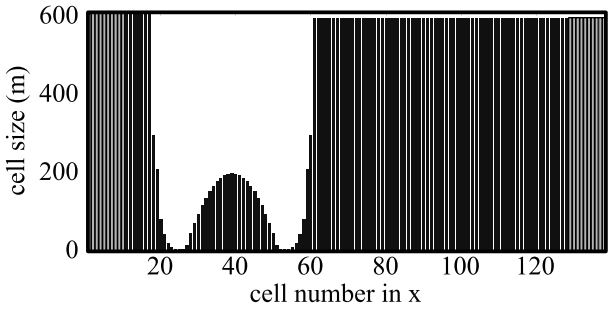

Figure 12. Nonuniform mesh in the $\hat{x}$ direction for the dual-transmitter pattern. The first element is 5 km from the edge of the space with inter-element spacing of $1/4\lambda$. The number of cells including PML layers $(x,y,z) = 138 \times 153 \times 100$. Black cells represent the computational domain, and gray cells represent the PML layers.

the resonant frequency point. Since the resonant frequency point provides a very stationary measurement across the highly variable weather conditions that exist at the South Pole, accurate predictions of this property by the simulation would constitute a validation of the numerical method.

[21] The computational space for the South Pole transmitter (not including PML layers) is $96 \times 133 \times 35$ cells representing a space which is $50 \times 50 \times 13.5$ km in dimension with $0 \leq x \leq 50$ km, $0 \leq y \leq 50$ km, and $-3.5 \leq z \leq 10$ km. Though the beacon is only 6.706 km in length, the space has been enlarged for the radiation resistance calculation which will be discussed later. The antenna is once again oriented in the $\hat{y}$ direction with a 4 m gap and is located 4 m above the ground. In this simulation, the antenna is excited with a broadband pulse of 100 kHz bandwidth modulated at 19.4 kHz. The nonuniform mesh for this case study is shown in Figure 5 and has the same PML configuration as the Siple Station simulation with only 5 PML layers below the bedrock and 10 layers in all other directions.

[22] Good agreement is obtained with the available data as shown in Figures 6a and 6b over the frequency band ranging from 10 to 21 kHz. Figure 6b represents an expanded portion of the impedance plot showing the resonance point in finer detail. The simulated resonant frequency is 19.5 kHz, which represents an error of less than 1% compared with the measured frequency of 19.4 kHz. The slopes of the resistance and reactance curves between the calculated and measured data sets exhibit some slight differences; however, it is important to note that the ice profile is not modified in any way to fit the data. We find through experimentation that small changes in the real and imaginary part of ϵ_r have little effect on the resulting input impedance. In other words, exact knowledge of the submerged ice is not necessary in order to obtain reasonable agreement with measured data over ice in the VLF frequency band. The calculated resistance value of 200 Ω at the resonant frequency compares well with the approximate value of 220 Ω measured over this range.

[23] Using our validated model we now calculate the radiation resistance, efficiency, and power pattern for the current South Pole beacon transmitter. The radiation resistance is calculated using equation (6) and solving for R_o:

$$\frac{1}{2}\mathcal{R}e \oint (\mathbf{E} \times \mathbf{H}^*) \cdot ds = \frac{1}{2} I^2 R_o, \tag{6}$$

where **E** and **H** are the Fourier transformed electric and magnetic fields, R_o is the radiation resistance, and I is the Fourier transformed terminal current as calculated in equation (5). The term on the left of equation (6) represents the total power flow exiting a closed imaginary surface near the outside of the computational domain located a few wavelengths from the antenna. This surface is placed two mesh points away from the PML in all directions, with the bottommost layer located in a horizontal slice plane through the bedrock. It is important that the Poynting vector flux be integrated at a location far enough away from the antenna so that all fields penetrating the ice have sufficiently attenuated and so that we can separate the radiated power from that which is absorbed into the ice through the near fields. Figure 7a shows the broadband radiation resistance, while Figure 7b represents an expanded region around the operating frequency of 19.4 kHz.

[24] With respect to Figure 7, the radiation resistance was found to be about 11 Ω. The efficiency was also calculated as shown in Figure 8. It can be deduced from the plots of the radiation resistance and efficiency that the ice absorbs much of the radiated power of the antenna, with the efficiency being only 7% at 19.4 kHz.

[25] For the power pattern calculation, the antenna is moved to within 5 km of the edge of the space since we are interested in how the energy is focused in the forward direction toward Palmer Station. A conceptual diagram depicting the simulation setup for this and the two-element case described in section 5 is shown in Figure 9.

[26] In Figure 9, $\hat{x}$ represents the direction along the ice toward Palmer Station, $\hat{y}$ represents the direction along the axis of the antenna, and $\hat{z}$ represents height above the surface of the ice. The PML layers which are not shown in Figure 9 are an extension of this space. The only major difference in the computational mesh used in the pattern calculation versus that of Figure 5 is that the antenna is located toward one side of the space in the $\hat{x}$ direction. The cell variation in $\hat{y}$ is unchanged, with the $\hat{z}$ direction

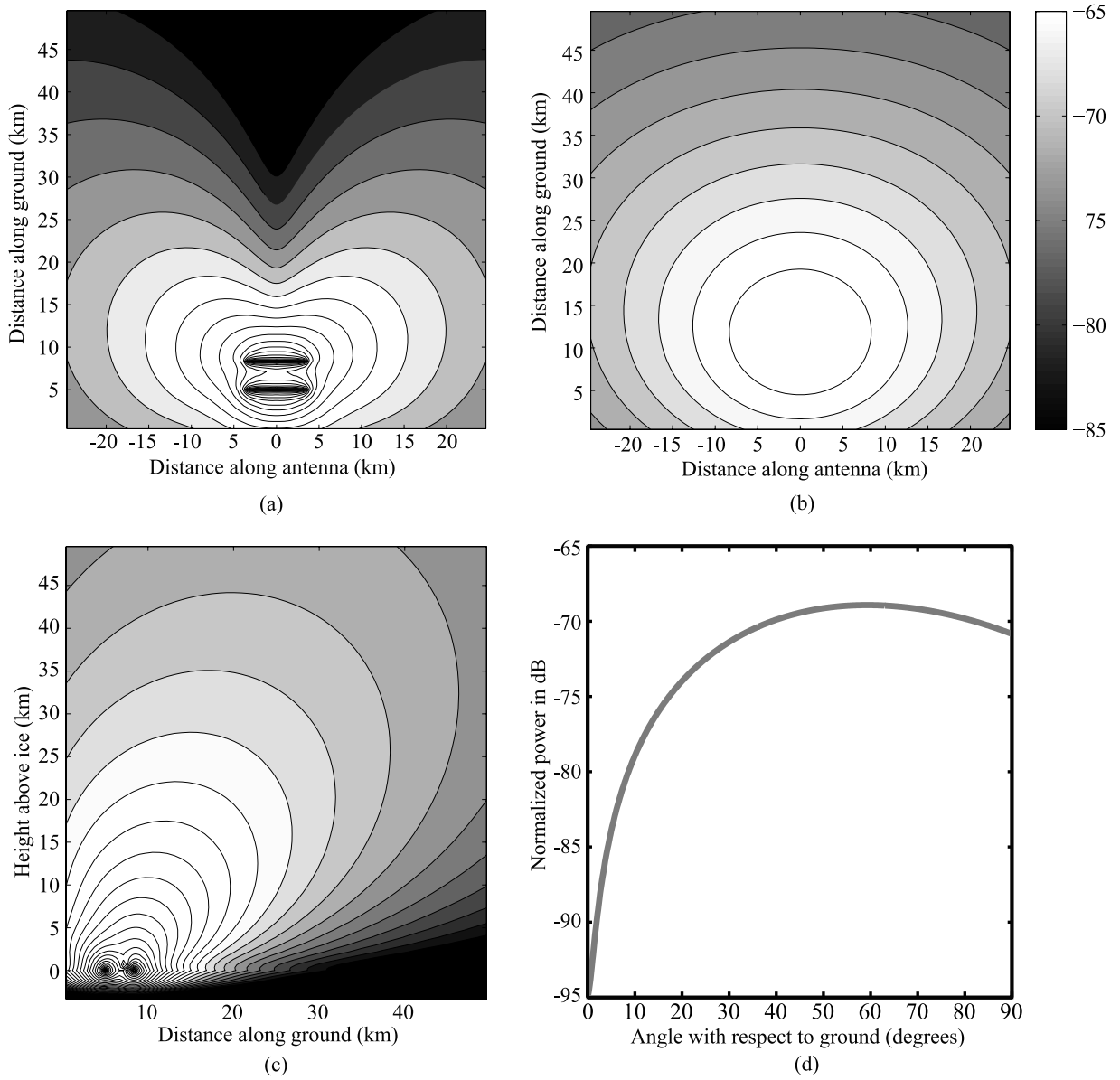

Figure 13. Normalized radiation pattern of the two-element phased array in dB. (a) Power pattern in the horizontal plane just above the ice surface. (b) Power pattern in the horizontal plane at 15 km altitude. (c) Power pattern in the vertical plane through antenna terminals. (d) Angular dependence of the power pattern at radial distance of 45 km from antenna terminals.

now extended to an altitude of 50 km with a maximum cell size of 800 m. The nonuniform mesh in the $\hat{x}$ direction is shown in Figure 10 with the PML layering and excitation characteristics unchanged from the previous case.

[27] The antenna pattern for the South Pole VLF transmitter in both horizontal and vertical planes is given in Figure 11. The pattern is calculated by taking the real part of a volumetric Fourier transform of the Poynting vector. Figure 11 represents the normalized power pattern of the antenna in dB realized as surfaces of constant power flux. Since the pattern is symmetric about the *xz* plane, the pattern is shown only for the direction facing Palmer Station, Antarctica.

[28] Figure 11a represents a horizontal slice through the antenna in the *xy* plane located 4 m above the surface. Figure 11b represents a horizontal slice in the *xy* plane at an altitude of 15 km. Figure 11c is a vertical slice of the power pattern in the *xz* plane taken through the terminals of the antenna, and Figure 11d is a plot of the power pattern as a function of angle ϕ between the ground and $\hat{z}$ axis. The power pattern in Figure 11d represents the pattern at a radius of 45 km from the terminals of the antenna. It can be seen from Figure 9 that the beam direction is focused vertically, thus launching less power toward Palmer Station.

5. Two-Antenna Study at the South Pole

[29] The final case study includes the modeling of a two-element VLF phased array to be located at the South Pole. Because of power limitations at the South Pole, it is assumed that the available input power for the two-dipole array would be the same as that for a single dipole. Two elements allow for more of the radiated power to be focused toward Palmer Station in an effort to increase the SNR of the received signal. This would enhance the study of ionospheric effects on guided wave propagation within the Earth-ionosphere waveguide. The goal of our numerical simulation is to determine the radiation properties of such a configuration.

[30] In this case, two transmitting antennas of length equal to the current transmitting antenna, spaced 1/4 of a wavelength apart and excited 90° out of phase with respect to each other, were modeled. The nonuniform mesh configuration differs from the single-element case only in the $\hat{x}$ direction, and this variation is shown in Figure 12.

[31] The PML layer configuration is identical to that of the single-transmitter case study. The radiation pattern of this two-element system is shown in Figure 13.

[32] It is seen in Figures 13c and 13d that the beam direction is now focused at an angle $\phi \approx 55°$ with respect to the horizontal ground plane. Thus more of the energy is focused in the forward direction toward Palmer with a gain of 3 dB in the beam direction over that of the single-transmitter case. The radiation resistance and efficiency were likewise calculated for the two-antenna system, but the plots were virtually indistinguishable from the single antenna configuration as one would expect: Although more power is being radiated, the antennas are driven with a proportionally larger amount of current into the same lossy dielectric; thus the radiation resistance (and hence the radiation efficiency) is unchanged.

6. Summary

[33] Previous estimates of the ice profile below the South Pole appear to be accurate with respect to the simulated and measured results of the input impedance. The measured input impedance is found to be relatively insensitive to small changes in the ice profile so that even coarser models may be used in the analysis of wave interaction problems over Antarctica. The ice profiles used in this work provide accurate results for the single-antenna case over two locations in Antarctica and have been successfully applied to a multiple-antenna system. The radiation characteristics for both single- and multiple-dipole elements have been calculated, and it has been shown that the two-element array is more efficient in transmitting energy into the Earth-ionosphere waveguide. This simulation model is shown to be a general and useful tool in the characterization of VLF transmitters over Antarctic ice.

[34] **Acknowledgment.** This research was supported under NSF grant NSF-OPP-0093381 and AFOSR grant F49620-03-1-0338.

References

Auty, R., and R. Cole (1952), Dielectric properties of ice and solid d2o, *J. Chem. Phys.*, *20*, 1309–1314.

Berenger, J.-P. (1994), A perfectly matched layer for the absorption of electromagnetic waves, *J. Comput. Phys.*, *114*(2), 185–200.

Carpenter, D., T. Bell, and A. Smith (1988), The Siple VLF transmitter as a multi-frequency probe of the Earth-ionosphere waveguide, *J. Atmos. Terr. Phys.*, *50*(2), 105–115.

Chevalier, M., and U. Inan (2004), A PML using a convolutional curl operator and a numerical reflection coefficient for general linear media, *IEEE Trans. Antennas Propag.*, *52*(7), 1647–1657.

Cotton, P. D., A. J. Smith, T. G. Wolf, W. L. Poulsen, and D. L. Carpenter (1992), The propagation of mixed polarization VLF ($F \leq 5$ kHz) radio waves in the Antarctic Earth-ionosphere waveguide, *Radio Sci.*, *27*(5), 593–610.

Gow, A., H. Ueda, and D. Garfield (1968), Antarctic ice sheet: Preliminary results of first core hole to bedrock, *Science*, *161*(3845), 1011–1013.

Helliwell, R., and J. Katsufrakis (1974), VLF wave injection into the magnetosphere from Siple Station, Antarctica, *J. Geophys. Res.*, *79*(16), 2511–2518.

Peden, I., and G. Webber (1970), Dielectric and loss properties of the Antarctic terrain: Their influence on the propagation constants of V.L.F. modes in the Earth-ionosphere waveguide, *IIEEE Trans. Antennas Propag.*, *18*(6), 840–842.

Peden, I., G. Webber, and A. Chandler (1972), Complex permittivity of the Antarctic ice sheet in the VLF band, *Radio Sci.*, *7*(6), 645–650.

Piket-May, M., A. Taflove, and J. Baron (1994), FD-TD modeling of digital signal propagation in 3-D circuits with passive and active loads, *IEEE Trans. Microwave Theory Tech.*, *42*(8), 1514–1523.

Raghuram, R., R. Smith, and T. Bell (1974), VLF Antarctic antenna: Impedance and efficiency, *IEEE Trans. Antennas Propag.*, *22*(2), 318–322.

Reynolds, J. (1985), Dielectric behaviour of firn and ice from the Antarctic peninsula, Antarctica, *J. Glaciol.*, *31*(109), 253–262.

Reznikov, A., A. Sukhorukov, D. Edemskii, V. Kopeikin, P. Morozov, B. Ryabov, A. Shchekotov, and V. Solov'ev (1993), Investigations of the lower ionosphere over Antarctic via ELF-VLF radiowaves, *Antarct. Sci.*, *5*(1), 107–113.

Rogers, J., and I. Peden (1975), VLF complex permittivity of deep Antarctic ice measured in situ, *Radio Sci.*, *10*(8–9), 763–771.

Taflove, A., and S. Hagness (2000), *Computational Electrodynamics: The Finite-Difference Time-Domain Method*, 2nd ed., Artech House, Norwood, Mass.

Thiel, D., and R. Mittra (1997), Surface impedance modeling using the finite-difference time-domain method, *IEEE Trans. Geosci. Remote Sens.*, *35*(5), 1350–1356.

Tkalcevic, S. (1983), Very-low frequency signals (2–10 kHz) received at Palmer Station, Antarctica, from the 21.4 km dipole antenna at Siple Station, 1400 km distant, *J. Atmos. Terr. Phys.*, *45*(6), 353–367.

Webber, G., and I. Peden (1971), VLF fields of a horizontal dipole below the polar anisotropic ionosphere, *IEEE Trans. Antennas Propag.*, *19*(4), 523–529.

Yee, K. (1966), Numerical solution of initial boundary value problems involving Maxwell's equations in isotropic media, *IEEE Trans. Antennas Propag.*, *14*(3), 302–307.

T. F. Bell, T. W. Chevalier, and U. S. Inan, Department of Electrical Engineering, Stanford University, 351 Packard EE Building, Stanford, CA 94103, USA. (timothyc@stanford.edu)